

# High-resolution fluorescence imaging via pattern-illuminated Fourier ptychography

Siyuan Dong,<sup>1,3</sup> Pariksheet Nanda,<sup>1,3</sup> Radhika Shiradkar,<sup>1</sup> Kaikai Guo,<sup>1</sup> and Guoan Zheng<sup>1,2\*</sup>

<sup>1</sup>Biomedical Engineering, University of Connecticut, Storrs, CT, 06269, USA

<sup>2</sup>Electrical and Computer Engineering, University of Connecticut, Storrs, CT, 06269, USA

<sup>3</sup>These authors contributed equally to this work

\*guoan.zheng@uconn.edu

<https://sites.google.com/site/gazheng/>

**Abstract:** Fluorescence microscopy plays a vital role in modern biological research and clinical diagnosis. Here, we report an imaging approach, termed pattern-illuminated Fourier ptychography (FP), for fluorescence imaging beyond the diffraction limit of the employed optics. This approach iteratively recovers a high-resolution fluorescence image from many pattern-illuminated low-resolution intensity measurements. The recovery process starts with one low-resolution measurement as the initial guess. This initial guess is then sequentially updated by other measurements, both in the spatial and Fourier domains. In the spatial domain, we use the pattern-illuminated low-resolution images as intensity constraints for the sample estimate. In the Fourier domain, we use the incoherent optical-transfer-function of the objective lens as the object support constraint for the solution. The sequential updating process is then repeated until the sample estimate converges, typically for 5-20 times. Different from the conventional structured illumination microscopy, any unknown pattern can be used for sample illumination in the reported framework. In particular, we are able to recover both the high-resolution sample image and the unknown illumination pattern at the same time. As a demonstration, we improved the resolution of a conventional fluorescence microscope beyond the diffraction limit of the employed optics. The reported approach may provide an alternative solution for structure illumination microscopy and find applications in wide-field, high-resolution fluorescence imaging.

©2014 Optical Society of America

**OCIS codes:** (170.2520) Fluorescence microscopy; (170.3010) Image reconstruction techniques; (100.3190) Inverse problems.

---

## References and links

1. J. Pawley, *Handbook of Biological Confocal Microscopy* (Springer, 2010).
2. M. G. Gustafsson, "Surpassing the lateral resolution limit by a factor of two using structured illumination microscopy," *J. Microsc.* **198**(2), 82–87 (2000).
3. M. G. Gustafsson, "Nonlinear structured-illumination microscopy: wide-field fluorescence imaging with theoretically unlimited resolution," *Proc. Natl. Acad. Sci. U.S.A.* **102**(37), 13081–13086 (2005).
4. M. G. Gustafsson, L. Shao, P. M. Carlton, C. J. Wang, I. N. Golubovskaya, W. Z. Cande, D. A. Agard, and J. W. Sedat, "Three-dimensional resolution doubling in wide-field fluorescence microscopy by structured illumination," *Biophys. J.* **94**(12), 4957–4970 (2008).
5. R. Heintzmann and M. G. Gustafsson, "Subdiffraction resolution in continuous samples," *Nat. Photonics* **3**(7), 362–364 (2009).
6. P. Kner, B. B. Chhun, E. R. Griffis, L. Winoto, and M. G. Gustafsson, "Super-resolution video microscopy of live cells by structured illumination," *Nat. Methods* **6**(5), 339–342 (2009).
7. E. Mudry, K. Belkebir, J. Girard, J. Savatier, E. Le Moal, C. Nicoletti, M. Allain, and A. Sentenac, "Structured illumination microscopy using unknown speckle patterns," *Nat. Photonics* **6**(5), 312–315 (2012).
8. A. Jost and R. Heintzmann, "Superresolution multidimensional imaging with structured illumination microscopy," *Annu. Rev. Mater. Res.* **43**(1), 261–282 (2013).

9. J. Min, J. Jang, D. Keum, S.-W. Ryu, C. Choi, K.-H. Jeong, and J. C. Ye, "Fluorescent microscopy beyond diffraction limits using speckle illumination and joint support recovery," *Sci. Rep.* **3**, 2075 (2013).
10. P. T. C. So, H.-S. Kwon, and C. Y. Dong, "Resolution enhancement in standing-wave total internal reflection microscopy: a point-spread-function engineering approach," *J. Opt. Soc. Am. A* **18**(11), 2833–2845 (2001).
11. J. García, Z. Zalevsky, and D. Fixler, "Synthetic aperture superresolution by speckle pattern projection," *Opt. Express* **13**(16), 6073–6078 (2005).
12. A. Gur, D. Fixler, V. Micó, J. García, and Z. Zalevsky, "Linear optics based nanoscopy," *Opt. Express* **18**(21), 22222–22231 (2010).
13. C. Ventalon and J. Mertz, "Quasi-confocal fluorescence sectioning with dynamic speckle illumination," *Opt. Lett.* **30**(24), 3350–3352 (2005).
14. C. Ventalon and J. Mertz, "Dynamic speckle illumination microscopy with translated versus randomized speckle patterns," *Opt. Express* **14**(16), 7198–7209 (2006).
15. C. Ventalon, R. Heintzmann, and J. Mertz, "Dynamic speckle illumination microscopy with wavelet prefiltering," *Opt. Lett.* **32**(11), 1417–1419 (2007).
16. Z. R. Hoffman and C. A. DiMarzio, "Structured illumination microscopy using random intensity incoherent reflectance," *J. Biomed. Opt.* **18**(6), 061216 (2013).
17. M. A. Neil, R. Juskaits, and T. Wilson, "Method of obtaining optical sectioning by using structured light in a conventional microscope," *Opt. Lett.* **22**(24), 1905–1907 (1997).
18. J. G. Walker and K. I. Hopcraft, "A diffuser-based optical sectioning fluorescence microscope," *Meas. Sci. Technol.* **24**(12), 125404 (2013).
19. D. Dan, M. Lei, B. Yao, W. Wang, M. Winterhalder, A. Zumbusch, Y. Qi, L. Xia, S. Yan, and Y. Yang, "DMD-based LED-illumination Super-resolution and optical sectioning microscopy," *Sci. Rep.* **3**, 1116 (2013).
20. K. Wicker, "Non-iterative determination of pattern phase in structured illumination microscopy using auto-correlations in Fourier space," *Opt. Express* **21**(21), 24692–24701 (2013).
21. R. Ayuk, H. Giovannini, A. Jost, E. Mudry, J. Girard, T. Mangeat, N. Sandeau, R. Heintzmann, K. Wicker, K. Belkebir, and A. Sentenac, "Structured illumination fluorescence microscopy with distorted excitations using a filtered blind-SIM algorithm," *Opt. Lett.* **38**(22), 4723–4726 (2013).
22. G. Zheng, R. Horstmeyer, and C. Yang, "Wide-field, high-resolution Fourier ptychographic microscopy," *Nat. Photonics* **7**(9), 739–745 (2013).
23. X. Ou, R. Horstmeyer, C. Yang, and G. Zheng, "Quantitative phase imaging via Fourier ptychographic microscopy," *Opt. Lett.* **38**(22), 4845–4848 (2013).
24. S. Dong, R. Horstmeyer, R. Shiradkar, K. Guo, X. Ou, Z. Bian, H. Xin, and G. Zheng, "Aperture-scanning Fourier ptychography for 3D refocusing and super-resolution macroscopic imaging," *Opt. Express* **22**(11), 13586–13599 (2014).
25. S. Dong, R. Shiradkar, P. Nanda, and G. Zheng, "Spectral multiplexing and coherent-state decomposition in Fourier ptychographic imaging," *Biomed. Opt. Express* **5**(6), 1757–1767 (2014).
26. G. Zheng, "Breakthroughs in photonics 2013: Fourier ptychographic imaging," *Photonics Journal, IEEE* **6**, 1–7 (2014).
27. G. Zheng, X. Ou, R. Horstmeyer, J. Chung, and C. Yang, "Fourier ptychographic microscopy: a gigapixel superscope for biomedicine," *Optics and Photonics News* **25**(4 April Issue), 26–33 (2014).
28. A. Williams, J. Chung, X. Ou, G. Zheng, S. Rawal, Z. Ao, R. Datar, C. Yang, and R. Cote, "Fourier ptychographic microscopy for filtration-based circulating tumor cell enumeration and analysis," *J. Biomed. Opt.* **19**(6), 066007 (2014).
29. R. Gerchberg, "A practical algorithm for the determination of phase from image and diffraction plane pictures," *Optik (Stuttg.)* **35**, 237 (1972).
30. J. R. Fienup, "Reconstruction of an object from the modulus of its Fourier transform," *Opt. Lett.* **3**(1), 27–29 (1978).
31. L. Taylor, "The phase retrieval problem," *Antennas and Propagation, IEEE Transactions on* **29**(2), 386–391 (1981).
32. J. R. Fienup, "Phase retrieval algorithms: a comparison," *Appl. Opt.* **21**(15), 2758–2769 (1982).
33. R. A. Gonsalves, "Phase retrieval and diversity in adaptive optics," *Opt. Eng.* **21**(5), 215829 (1982).
34. B. H. Dean and C. W. Bowers, "Diversity selection for phase-diverse phase retrieval," *J. Opt. Soc. Am. A* **20**(8), 1490–1504 (2003).
35. C.-H. Lu, C. Barsi, M. O. Williams, J. N. Kutz, and J. W. Fleischer, "Phase retrieval using nonlinear diversity," *Appl. Opt.* **52**(10), D92–D96 (2013).
36. H. M. L. Faulkner and J. M. Rodenburg, "Movable aperture lensless transmission microscopy: a novel phase retrieval algorithm," *Phys. Rev. Lett.* **93**(2), 023903 (2004).
37. M. Guizar-Sicairos and J. R. Fienup, "Phase retrieval with transverse translation diversity: a nonlinear optimization approach," *Opt. Express* **16**(10), 7264–7278 (2008).
38. X. Ou, G. Zheng, and C. Yang, "Embedded pupil function recovery for Fourier ptychographic microscopy," *Opt. Express* **22**(5), 4960–4972 (2014).
39. P. Thibault, M. Dierolf, O. Bunk, A. Menzel, and F. Pfeiffer, "Probe retrieval in ptychographic coherent diffractive imaging," *Ultramicroscopy* **109**(4), 338–343 (2009).
40. F. Hüe, J. M. Rodenburg, A. M. Maiden, and P. A. Midgley, "Extended ptychography in the transmission electron microscope: Possibilities and limitations," *Ultramicroscopy* **111**(8), 1117–1123 (2011).

- 
41. Z. Bian, S. Dong, and G. Zheng, "Adaptive system correction for robust Fourier ptychographic imaging," *Opt. Express* **21**(26), 32400–32410 (2013).
  42. S. Dong, Z. Bian, R. Shiradkar, and G. Zheng, "Sparsely sampled Fourier ptychography," *Opt. Express* **22**(5), 5455–5464 (2014).
- 

## 1. Introduction

The lateral resolution of conventional fluorescence microscopy is determined by the diffraction limit of the employed optics:  $\lambda/(2NA_{\text{obj}})$ , where  $\lambda$  is the wavelength of the incidence and  $NA_{\text{obj}}$  is the numerical aperture (NA) of the objective lens [1]. This diffraction limit, however, is established under the assumptions of single image acquisition and uniform light illumination. It is possible to combine multiple acquisitions with non-uniform illuminations to bypass this resolution barrier. Frequency mixing between the sample and the non-uniform illumination pattern shifts the high-frequency components to the passband of the collection optics. Therefore, the recorded image contains sample information that is beyond the diffraction limit. Structured illumination microscopy (SIM) is one good example towards this end [2–10]. A typical SIM setup projects a sinusoidal pattern at the sample plane and uses at least three phase steps to laterally shift the pattern across the sample. The corresponding images will be used to improve the resolution along the orthogonal direction of the sinusoidal pattern. Following a similar logic, sinusoidal patterns with other orientations will be used to improve the resolution along other directions. In the linear regime, the SIM approach is able to improve the diffraction-limited resolution by a factor of two, and thus, the final achievable NA can be twice of the objective's NA. The capability of bypassing diffraction limit has made SIM a popular tool for super-resolution fluorescent imaging.

In this paper, we report a novel fluorescence imaging approach, termed pattern-illuminated Fourier ptychography (FP), for bypassing the diffraction limit of the employed optics. Similar to SIM and other speckle illumination schemes [2–21], the reported approach uses non-uniform intensity patterns for sample illumination and acquires the corresponding diffraction-limited intensity images. Based on the acquired images, a novel Fourier ptychographic recovery algorithm is used to reconstruct the high-resolution sample image in an iterative manner. The recovery process starts with a low-resolution intensity image as the initial guess. This initial guess is then sequentially updated by other low-resolution measurements taken under different illumination patterns. Similar to the original FP approach [22–28], the iterative updating process also switches between the spatial and Fourier domains. In the spatial domain, we use the pattern-illuminated low-resolution images as intensity constraints for the sample estimate. In the Fourier domain, we use the incoherent optical-transfer-function of the objective lens as the object support constraint for the solution. This sequential updating process is iterated until the sample estimate converges (5–20 times).

We note that, the strategy of using non-uniform illumination for improving lateral or axial resolution is not new [2–21]. However, the use of the FP framework [22–28] to recover a high-resolution fluorescence image is new and may provide an alternative solution to existing SIM and speckle illuminating platforms. As the use of fluorescence microscopy is prolific in modern biological research and clinical diagnosis [1], the reported approach may open up new opportunities for the Fourier ptychographic imaging paradigm.

This paper is structured as follows: in section 2, we will outline the pattern-illuminated FP approach and its recovery procedures. In section 3, we will validate the reported algorithm using simulations. In section 4, we will demonstrate the implementation of the reported approach on a conventional epi-illumination fluorescence microscope. We will show that, the reported approach is able to improve the lateral resolution beyond the diffraction limit of the employed optics. Finally, we will summarize the results and discuss the future directions.

## 2. Pattern-illuminated Fourier ptychography

Fourier ptychography (FP) is a coherent imaging technique that uses angle-varied illumination for high-resolution complex image recovery [22–28]. The previously reported FP instrument used an LED array for sample illumination and a low-NA objective lens for image acquisition. Each LED element of the array illuminates the sample from an oblique incident angle and the corresponding image is acquired using the low-NA objective lens. These acquired images are then synthesized in the Fourier space to produce a high-resolution complex sample image that surpasses the diffraction limit of the objective lens. In the recovery process, FP switches between the spatial and Fourier domains. In the spatial domain, the acquired images are used to constrain the amplitude of the solution, similar to the strategy of the phase retrieval technique [29–37]. In the Fourier domain, the coherent transfer function (i.e., the pupil function) of the objective is used as a support constraint for the solution. This support constraint is digitally panned across the Fourier space to reflect the angle-varied illuminations. Essentially, the FP approach combines the phase retrieval technique and the synthetic aperture concept to recover the phase information and expand the Fourier passband at the same time. It has been shown that FP is able to recover a high-resolution complex image with a large field-of-view using a low-NA objective lens. The recovered phase information of 2D thin samples is shown to be quantitative in nature [23].

As a coherent imaging technique, the original FP approach cannot be used for fluorescence microscopy. The reason is very simple: fluorophores are not responsive to phase variation of the excitation waves. In the original FP prototype, no matter which angle we illuminate the sample, the fluorescence emission remains unchanged and no additional information can be extracted from the raw images. To modify the FP recovery concept for fluorescence microscopy, we can simply replace the plane wave illuminations with intensity-varied patterns. In this case, fluorophores are responsive to the intensity variations, and each low-resolution image provides additional information for the high-resolution sample profile. We term such a scheme as pattern-illuminated Fourier ptychography.

As shown in Fig. 1, the pattern-illuminated FP approach uses multiple intensity-varied pattern  $P_n$  ( $n = 1,2,3\dots$ ) to illuminate the object  $I_{obj}$  and acquires the corresponding low-resolution images  $I_n$  ( $n = 1,2,3\dots$ ) through the objective lens. The proposed algorithm aims to recover the high-resolution object image  $I_{obj}$  from the low-resolution images  $I_n$  ( $n = 1,2,3\dots$ ). Here we assume that the illumination pattern  $P_n$  is known. Later in this section, we will extend the recovery framework for an unknown illumination pattern.

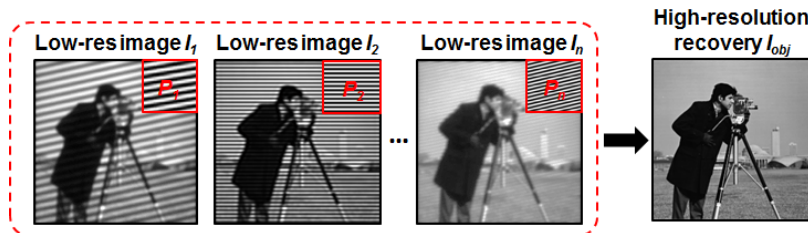


Fig. 1. Overview of the pattern-illuminated FP recovery scheme. Multiple pattern-illuminated low-resolution images  $I_n$  ( $n = 1,2,3\dots$ ) are used to recover the high-resolution sample image  $I_{obj}$ . In the last low-resolution image  $I_n$ , the high-frequency illumination pattern is filtered out by the low-NA objective lens.

The image formation process can be expressed in Fourier space as follows:

$$\mathcal{F}(I_n) = OTF \cdot \mathcal{F}(I_{obj} \cdot P_n), \quad (1)$$

where  $\mathcal{F}()$  denotes the Fourier transform of the image, and  $OTF$  denotes the incoherent optical-transfer-function of the low-NA objective lens. There are two multiplication steps in Eq. (1): one in the spatial domain and one in the Fourier domain. In the spatial domain, the object emission profile is multiplied with the illumination pattern to produce a target image:  $I_m = I_{obj} \cdot P_n$ . In the Fourier domain, the incoherent OTF is multiplied with the spectrum of the target image to produce the spectrum of the measurement:  $\mathcal{F}(I_n) = OTF \cdot \mathcal{F}(I_{obj} \cdot P_n)$ . To recover the high-resolution object emission profile,  $I_{obj}$ , we need to invert these two multiplication steps in both the spatial and Fourier domains.

A flow chart of the recovery algorithm is shown in Fig. 2. It starts with an initial guess of the sample emission profile (step 1). This initial guess is sequentially updated by other low-resolution measurements taken under different illumination patterns (step 2). The updating process is iterated until the solution converges (step 3).

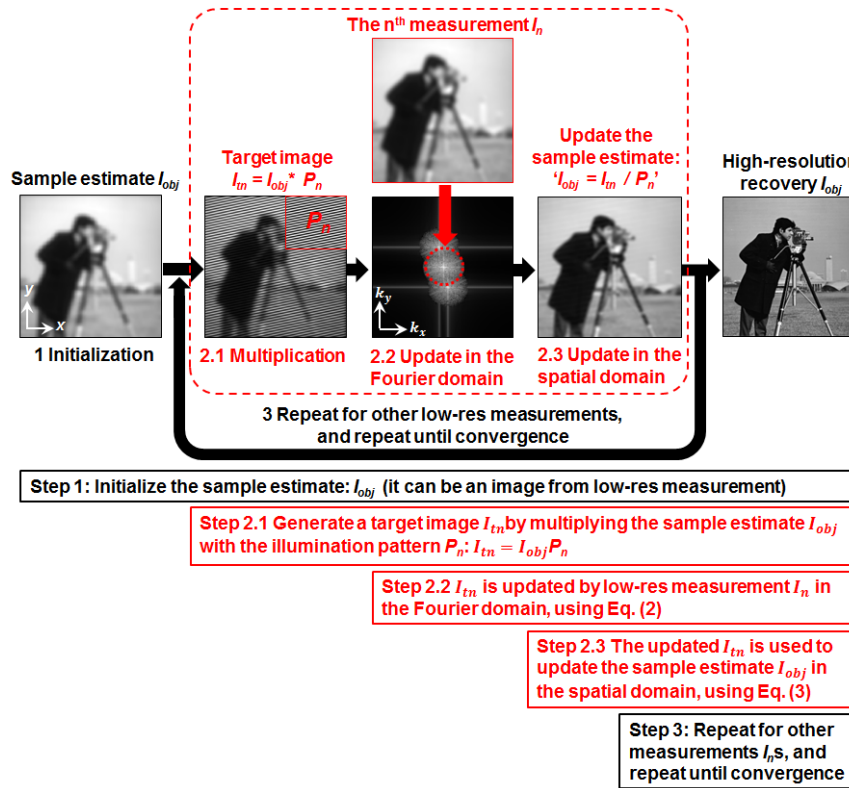


Fig. 2. Flow chart of the pattern-illuminated FP algorithm.

These three steps can be explained in details as follows: Step 1: it starts with an initial guess of the sample emission profile,  $I_{obj}$ . This initial guess can either be an interpolation of one low-resolution measurement or a random guess. Step 2.1: the initial guess is then multiplied with the illumination pattern,  $P_n$ , to produce a target image,  $I_m$ , in the spatial domain:  $I_m = I_{obj} \cdot P_n$ . Step 2.2: the target image,  $I_m$ , is updated by the low-resolution measurement,  $I_n$ , in the Fourier space as follows:

$$\mathcal{F}(I_m)^{updated} = \mathcal{F}(I_m) + OTF \cdot (\mathcal{F}(I_n) - OTF \cdot \mathcal{F}(I_m)) \quad (2)$$

The term  $\mathcal{F}(I_m)^{updated}$  is then transformed back to the spatial domain to produce an updated target image,  $I_m^{updated}$ . Step 2.3: the updated target image,  $I_m^{updated}$ , is then used to update the high resolution sample estimate in the spatial domain using the following equation:

$$I_{obj}^{updated} = I_{obj} + \frac{P_n}{(\max(P_n))^2} \cdot (I_m^{updated} - I_{obj} \cdot P_n) \quad (3)$$

Step 3: The updating process is repeated for all different illumination patterns and iterated until the solution converges. The convergence metric is the mean-square-error (MSE) of two consecutively recovered solutions. The process stops if the MSE is smaller than a pre-defined value.

We note that, Eq. (2) is performed in the Fourier domain and Eq. (3) is performed in the spatial domain. Similar procedures can also be found in the pupil recover scheme of the original FP approach [38], as well as in the conventional ptychography approach [39, 40]. In conventional SIM platforms, the illumination patterns are generated by two beam interference and, thus, the patterns are known. In this case, Eq. (2)-(3) can be used to recover the high-resolution sample image. We note that, unlike the conventional SIM recovery scheme, the reported algorithm requires no phase stepping of the sinusoidal pattern.

It is straight forward to extend the reported framework for handling an unknown pattern. In this case, one unknown pattern can be used to generate multiple low resolution images by projecting the pattern at different spatial positions or rotating it for different orientations. For each pattern projection, one low-resolution image is acquired using the low-NA objective lens. Similar to the recovery process of the sample image,  $I_{obj}$ , we can assign an initial guess for the unknown pattern,  $P_{unknown}$ . In our implementation, we use uniform illumination (i.e.,  $P_{unknown} = 1$ ) as the initial guess. To recover this unknown pattern, we only need to add one sub-step, step 2.4, in the image updating process. In this sub-step, the updated target image,  $I_m^{updated}$ , is used to update the unknown pattern as follows:

$$P_{unknown}^{updated} = P_{unknown} + \frac{I_{obj}}{(\max(I_{obj}))^2} \cdot (I_m^{updated} - I_{obj} \cdot P_{unknown}(x - x_n)), \quad (4)$$

where  $x_n$  is the scanning position of the sample (or the unknown pattern).

We note that, the use of translated illumination pattern has been demonstrated by Ventalon and Mertz for improving the axial resolution of fluorescence microscopy [14]. Our work, on the other hand, uses the translated illumination pattern to improve the lateral resolution of the sample emission profile. Furthermore, the reported recovery algorithm does not rely on the statistical nature of the illumination patterns. The iterative algorithm is able to recover both the high-resolution sample image and the unknown pattern at the same time.

### 3. Simulations of the pattern-illuminated FP framework

We first simulated the use of the reported framework for conventional SIM system, where the known sinusoidal patterns are used for sample illumination. Figure 3(a1) shows the simulated raw image acquired by a 0.15 NA objective lens (0.25  $\mu\text{m}$  pixel size). Figure 3(a2) shows the same raw image with 1% additive Gaussian noise. Figure 3(a3) shows the corresponding Fourier spectrum of the raw image.

Next, we used different numbers of sinusoidal patterns for sample illumination and perform image recovery using the pattern-illuminated FP algorithm. In Fig. 3(b), we use 18 sinusoidal patterns for illumination. We only changed the orientations of the sinusoidal patterns and no phase stepping was needed. The frequency of the sinusoidal patterns

corresponds to an illumination NA of 0.1. In Fig. 3(c), we use 36 sinusoidal patterns with two different frequencies. The frequency of the first 18 patterns corresponds to an illumination NA of 0.1, and the frequency of the other 18 patterns corresponds to an illumination NA of 0.25. Therefore, the cutoff frequency of the final recovered image in Fig. 3(c) is improved by 0.25 NA. Following a similar logic, we use 54 sinusoidal patterns in Fig. 3(d), corresponding to three different illumination NAs (0.1, 0.25, and 0.4). The cutoff frequency of the final recovered image shown in Fig. 3(d) is, therefore, improved by 0.4 NA. We also study the noise performance of the proposed algorithm by adding different amounts of Gaussian noise to the raw image. Figures 3(b2)-3(d2) demonstrate the recovered images with 1% additive noise. Figure 3(e) shows the MSE as a function of different noise levels. We can see that the image quality degrades linearly as a function of the additive noise. Therefore, the reported framework is robust against additive noises.

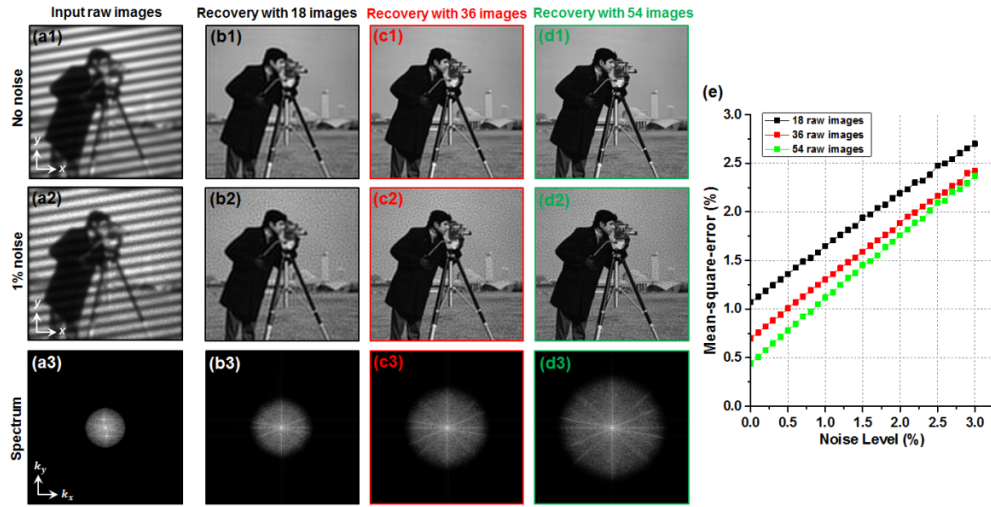


Fig. 3. Pattern-illuminated FP recovery using sinusoidal patterns. (a1) Simulated raw image without noise, and (a2) with 1% additive noise. (a3) The Fourier spectrum of (a1). FP recoveries using (b) 18 raw images, (c) 36 images, and (d) 54 images. We used 15 loops for the FP reconstructions. For the noise-free cases, the corresponding MSEs are 1.07%, 0.70%, and 0.44% for (b1)-(d1). For the cases with 1% noise, the corresponding MSEs are 1.65%, 1.30%, and 1.12% for (b2)-(d2). (e) The MSE is plotted as function of different noise levels. Different color lines correspond to different number of raw images.

To clearly demonstrate the resolution enhancement using the reported scheme, we performed a set of simulations using the star resolution pattern in Fig. 4. Figure 4(a) shows the diffraction-limited image using a 0.15 NA objective lens. Figure 4(b) shows the deconvolved image of Fig. 4(a). Figures 4(c) and 4(d) show the FP reconstructions using 36 and 54 raw images, with the same simulation setting as Fig. 3(c) and 3(d). The resolution enhancement is evident both in the spatial and the Fourier domain. The resolution enhancement effect is essentially the same as the SIM. Frequency mixing between the sample and the non-uniform illumination pattern shifts the high-frequency components to the passband of the collection optics. Therefore, the recorded image contains sample information that is beyond the NA of the employed lens. The reported FP scheme iteratively re-distributes this information into the corresponding regions in the Fourier space.

We also analyze the effect of rotation error and background level in Fig. 5. In this set of simulations, we used 54 raw images for FP reconstructions, same as Fig. 4(d). Figures 5(a1)-5(a3) show the recovered images with 0%, 1%, and 10% rotation errors of the sinusoidal patterns. The corresponding MSEs are 0.35%, 0.92%, and 1.07%. Figures 5(b1)-5(b3) show the recovered images with 0%, 10%, and 100% backgrounds. The corresponding MSEs are

0.35%, 0.68%, and 10.2%. From this set of simulations, we can see that, the reported scheme is robust against rotational error and auto-fluorescence background level.

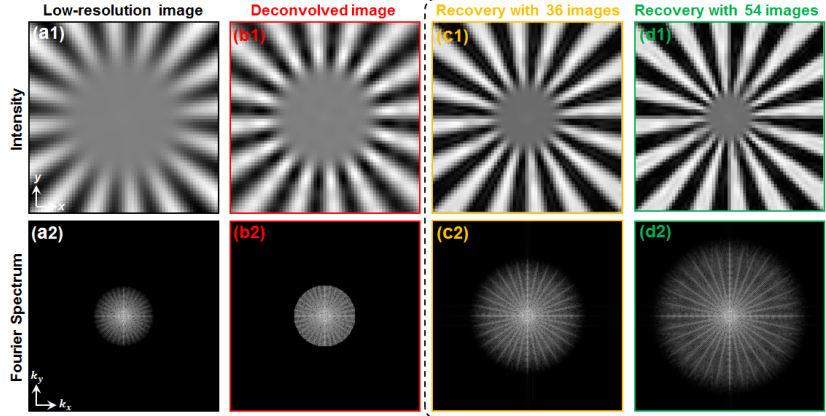


Fig. 4. Demonstration of resolution enhancement using a star image. (a1) Simulated diffraction-limited low-resolution image. (b1) Deconvolved image of (a1). The FP reconstructions using 36 (c1) and 54 (d1) raw images. (a2-d2) The Fourier spectrum of (a1-d1). We used 15 loops for the FP reconstructions and the corresponding MSEs are 0.64% and 0.35% for (c1) and (d1).

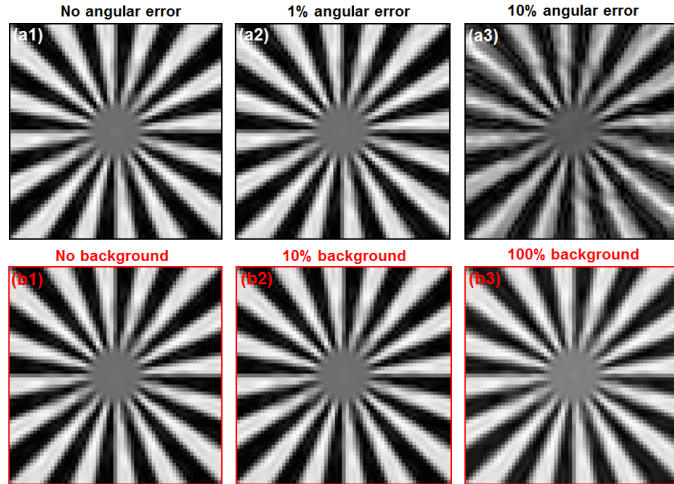


Fig. 5. Effect of rotational error and background level with sinusoidal illumination patterns. The FP recovered images with (a1) 0%, (a2) 1%, and (a3) 10% rotation errors. The corresponding MSEs are 0.35%, 0.92%, and 1.07%. The FP recovered images with (b1) 0%, (b2) 10%, and (b3) 100% backgrounds. The corresponding MSEs are 0.35%, 0.68%, and 10.2%.

In a practical experiment, it is difficult to precisely characterize the illumination pattern. Therefore, it is important to extend the reported FP framework to handle unknown illumination patterns. As we have discussed in the section 2, we can use one unknown pattern in our framework and translate this pattern to different spatial positions for sample illumination (the scanning step needs to be at the same scale of the speckle size). The object and the unknown pattern can be updated using Eq. (3) and Eq. (4) in the iterative recovery process.

In Fig. 6, we simulated the case of translating one unknown speckle pattern to 169 different spatial positions for sample illumination. The simulated raw images are shown in

Fig. 6(b). The recovered unknown illumination pattern and object image are shown in Fig. 6(c) and 6(d). The MSE of Fig. 6(d1) is 0.4%, comparable to the case of Fig. 3(d1). We note that, the unknown speckle pattern in this simulation is fully randomized. Therefore, the upper frequency limit of the pattern, shown in Fig. 6(a), is only determined by the employed pixel size. In a practical experimental setting, the upper frequency limit for the speckle pattern is, however, determined by the employed optics. For example, if a 0.9 NA condenser is used to focus the speckle pattern onto the sample, the maximum NA of the speckle pattern is 0.9. The corresponding frequency support constraint can then be imposed for illumination pattern at each iteration loop (the components outside the frequency support constraint are set to zero).

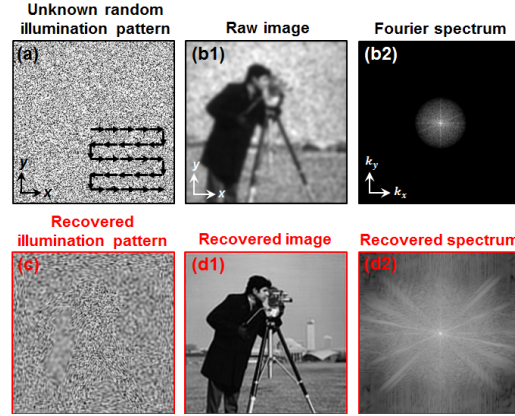


Fig. 6. Pattern-illuminated FP recovery using unknown illumination patterns. (a) The unknown illumination pattern (random pattern) is translated into 169 different spatial positions. (b1) The simulated raw image. (b2) The Fourier spectrum of (b1). (c) The recovered illumination pattern. (d) The recovered high-resolution object image and its Fourier spectrum. We used 15 loops for the FP reconstructions. The MSE of (d1) is 0.4%.

In Fig. 7, we used the star resolution image and one translating unknown speckle pattern for FP reconstruction (the simulation setting is the same as Fig. 6). Figure 7(a) shows the diffraction-limited image using a 0.15 NA objective lens. Figure 7(b) shows the deconvolved image of Fig. 7(a). Figures 7(c1) and (c3) show the FP reconstructions for both the high-resolution sample image and the unknown pattern. The MSE of Fig. 7(c1) is 0.32%, similar to that of Fig. 6(d1).

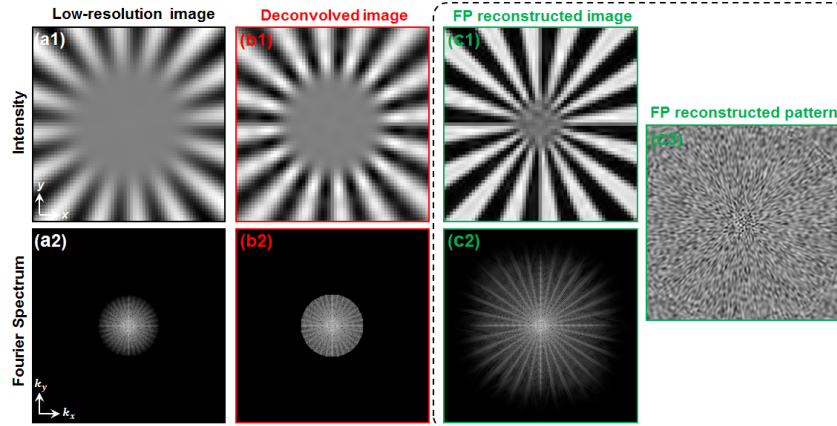


Fig. 7. Demonstration of resolution enhancement using a star image. (a1) Simulated diffraction-limited low-resolution image. (b1) Deconvolved image of (a1). (c) The FP reconstructions using by translating one unknown speckle pattern to 169 different spatial positions. We used 15 loops for the FP reconstructions and the MSE of (c1) is 0.32%.

In Fig. 8, we analyze the effect of positional error and background level for the FP reconstructions (the simulation setting is the same as Fig. 6). Figures 8(a1) and 8(a3) show the FP recovered images with 0%, 1%, and 10% positional errors of the unknown speckle pattern. The corresponding MSEs are 0.32%, 0.41%, and 10.7%. Figures 8(b1) and 8(b3) show the recovered images with 0%, 10%, and 100% uniform backgrounds, and the MSEs are 0.32%, 0.64%, and 10.2%, respectively.

In Fig. 9, we analyze the effect of additive noise (the simulation setting is the same as Fig. 6). Different amounts of Gaussian noises are added into the simulated raw images. The reconstructed FP images are shown in Fig. 9(b1) and (b3). The corresponding MSEs are 0.55%, 0.63%, and 1.57%, respectively.

Finally, we also study the effect of high-pass filtered pattern in Fig. 10. Figure 10(a) demonstrates the case of random speckle illumination where the spectrum amplitude covers all regions of the Fourier space. In Fig. 10(b), we simulated the case of high-pass speckle amplitude (Fig. 10(b2)), and the corresponding intensity pattern contains more high-frequency components (Fig. 10(b1)). Figure 10(a3) and 10(b3) show the corresponding FP reconstructions, and their MSEs are 0.32% and 0.38%. We note that, the design of optimal speckle spectrum for the reported FP scheme is an interesting topic and further investigation is needed.

The simulations shown in Fig. 3-10 validate the effectiveness and robustness of the reported pattern-illuminated FP recovery algorithm.

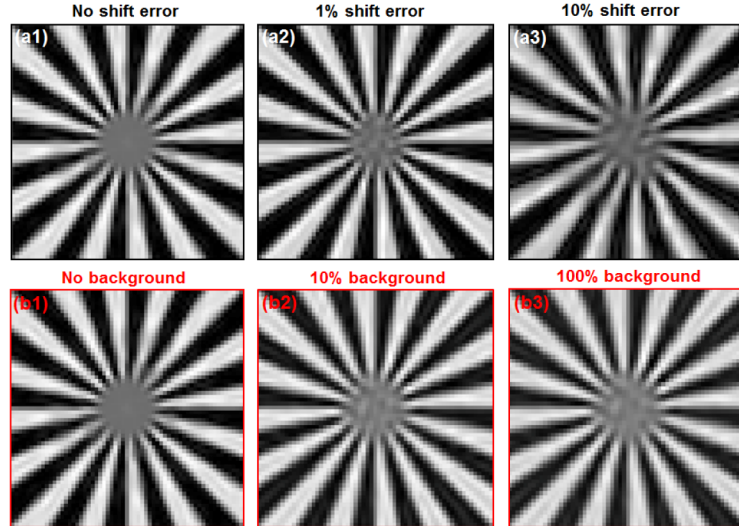


Fig. 8. Effect of positional error and background level with one translating unknown illumination pattern. The FP recovered images with (a1) 0%, (a2) 1%, and (a3) 10% positional errors. The corresponding MSEs are 0.32%, 0.41%, and 10.7%. The FP recovered images with (b1) 0%, (b2) 10%, and (b3) 100% backgrounds. The corresponding MSEs are 0.32%, 0.64%, and 10.2%.

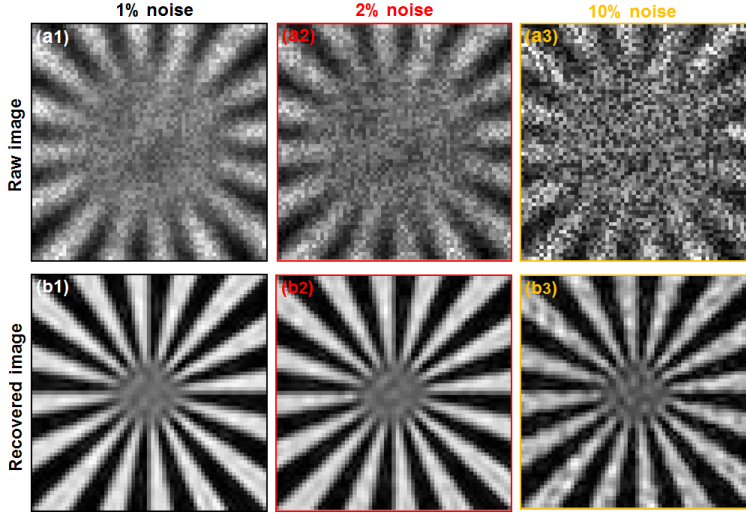


Fig. 9. Effect of additive noises with one translating unknown illumination pattern. (a1)-(a3) Raw images with 1%, 2%, and 10% additive Gaussian noise. (b1)-(b3) The corresponding FP reconstructions. The corresponding MSEs are 0.55%, 0.63%, and 1.57%.

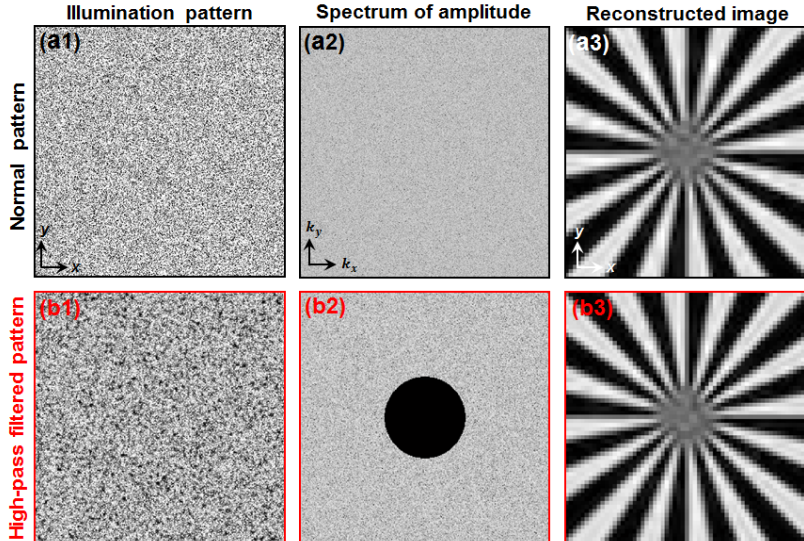


Fig. 10. Comparison between (a) random speckle pattern and (b) high-pass speckle pattern for sample illumination. The MSEs of (a3) and (b3) are 0.32% and 0.38%.

#### 4. Experimental demonstration of the pattern-illuminated FP approach

In this section, we will use the reported framework to improve the resolution of a commercially available fluorescence microscope (Nikon Ti-E motorized microscope). The experimental setup is shown in Fig. 11, where a 488 nm laser diode is used as light source and a diffuser is inserted into the epi-illumination reflector cube. The excitation light, thus, forms a random speckle pattern on the sample. The resulting fluorescence emission then passes through the detection path and reaches the CCD sensor. To acquire a pattern-illuminated FP data set, we only need to move the sample to different spatial positions using the motorized XY stage and acquire the corresponding fluorescence images. We note that, our setup is compatible with most existing epi-illuminated microscope platforms; no major hardware

modification is needed besides adding the diffuser to the excitation filter position of the reflector cube.

In our demonstration, we used a mouse kidney section (Molecular Probes F24630, Life Technology) as our sample. The central wavelength of the emission filter is 525 nm, with a 50 nm bandwidth (Semrock FF03-525/50-25). We use a 10X 0.25 NA objective lens (Nikon) and a CCD camera (Andor Clara CCD) for image acquisition. The sample is moved to 49 different positions in our experiment, and the acquired images are used to recover both the high-resolution sample emission profile and the unknown illumination pattern. Figures 11(b1) and (b4) demonstrate 4 out of 49 acquired raw images using the reported platform. As expected, we can clearly see the speckle-like features from these raw images. We note that, the 10X, 0.25 NA objective lens is used both for illumination and light collection in the reported setting. Therefore, the upper frequency limit of the speckle pattern is determined by the incoherent optical-transfer-function of the 0.25 NA lens. In the recovery process, we imposed the corresponding frequency support to constrain the illumination pattern at each iteration loop.

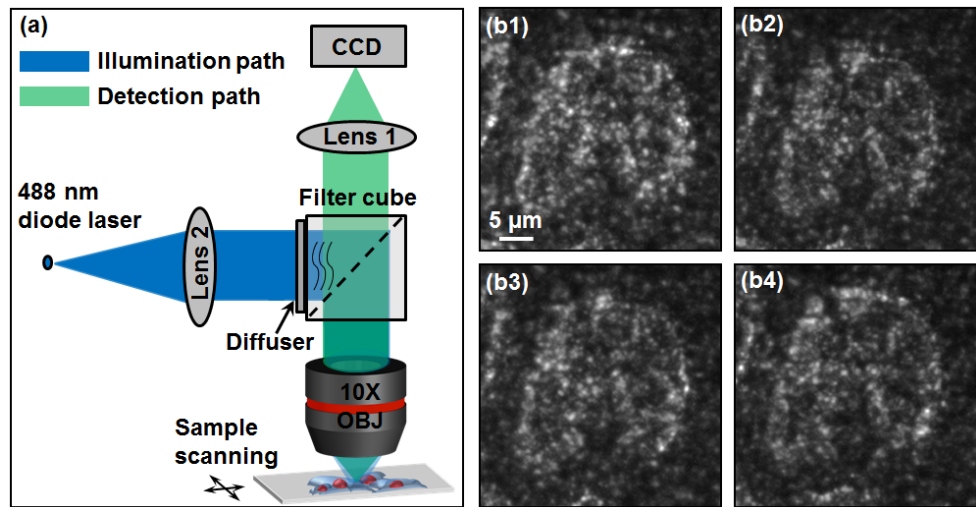


Fig. 11. (a) Pattern-illuminated FP setup. A diffuser is placed at the epi-illuminated arm of the microscope platform. The excitation light from the objective lens forms a speckle pattern on the sample. The resulting fluorescence emission from sample is then collected by the objective lens and detected by the CCD camera. (b1)-(b4) 4 acquired raw images.

Figure 12 demonstrates the performance of the pattern-illuminated FP approach. In Fig. 12(a1), we use the same 10X objective lens with uniform illumination to capture the sample image. The deconvolved image of Fig. 12(a1) is shown in Fig. 12(a2). Figure 12(b1) shows the raw FP image using the speckle illumination. Figure 12(b2) shows the FP reconstruction using 49 raw images. Figure 12(c1) shows the image captured by a 40X high-NA objective lens using uniform illumination. Figures 12(a3), 12(b3), and 12(c2) show the intensity line traces of a small feature of the sample, corresponding to the highlighted regions of Fig. 12(a1), 12(a2), 12(b2) and 12(c1). As shown in Fig. 12(a2), we cannot resolve the two lines using the 10X objective lens. We can, however, barely resolve the two-line feature using the FP recovered image in Fig. 12(b2). We also observe the same feature from the image captured by the 40X high-NA objective lens in Fig. 12(c). Therefore, from the comparison of this set of images, we verify that the observed two-line feature is not an artifact of the FP reconstruction process. From Fig. 12(b) and 12(c), the distance between these two lines is estimated to be 0.66 μm. By resolution criteria, the NA of the FP recovered image is, thus,

determined to be  $\sim 0.44$ . The corresponding resolution enhancement factor is  $\sim 1.8$ , close to the theoretical limit of 2.

We further compare the FP reconstructions using different numbers of raw images in Fig. 13. Figures 13(a)-13(d) show FP reconstructions using 9, 16, 25, and 49 frames respectively. From this comparison, we can see that, the FP reconstruction converges with 25 raw images.

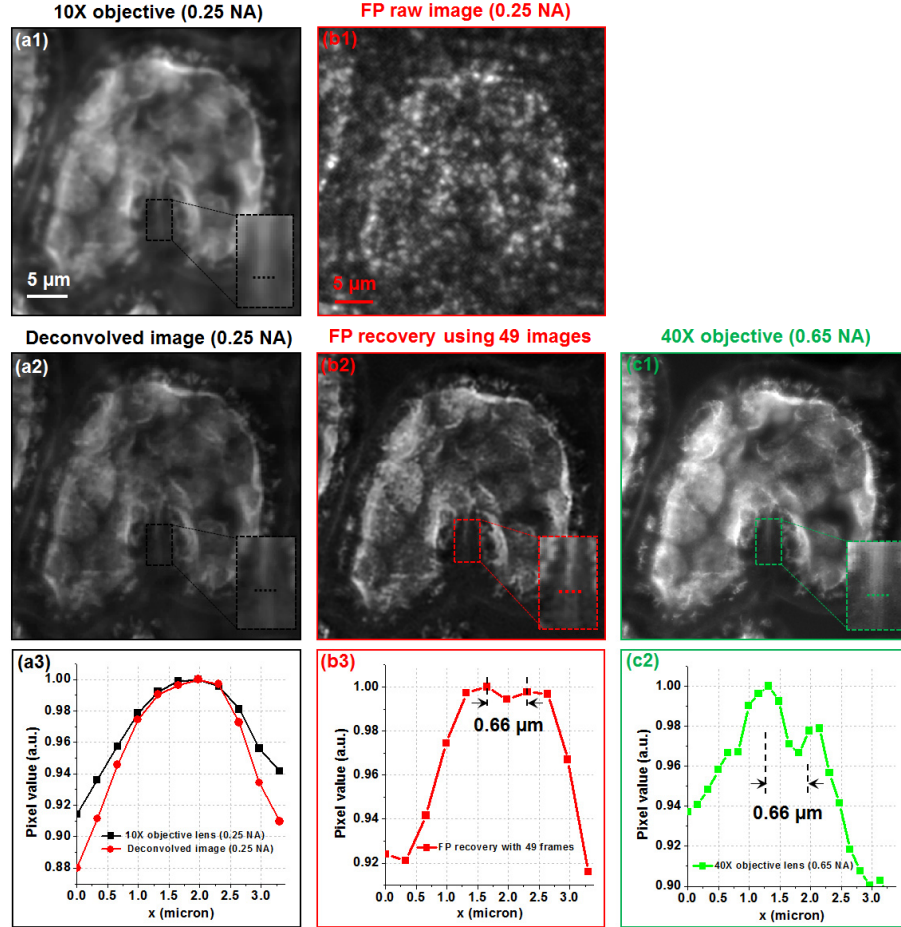


Fig. 12. Experimental demonstration of the pattern-illuminated FP approach. (a1) Sample image acquired using the 10X objective with uniform illumination. (a2) Deconvolved image of (a1). (b1) Speckle-illuminated FP raw image. (b2) FP recovery using 49 raw images. (c1) Sample image acquired using a 40X high-NA objective. (a3), (b3), (c2) Intensity line traces of the highlighted features in (a1), (a2), (b2), and (c1). For (a1) and (c1), we averaged multiple frames to get a similar photon budget as (b2).

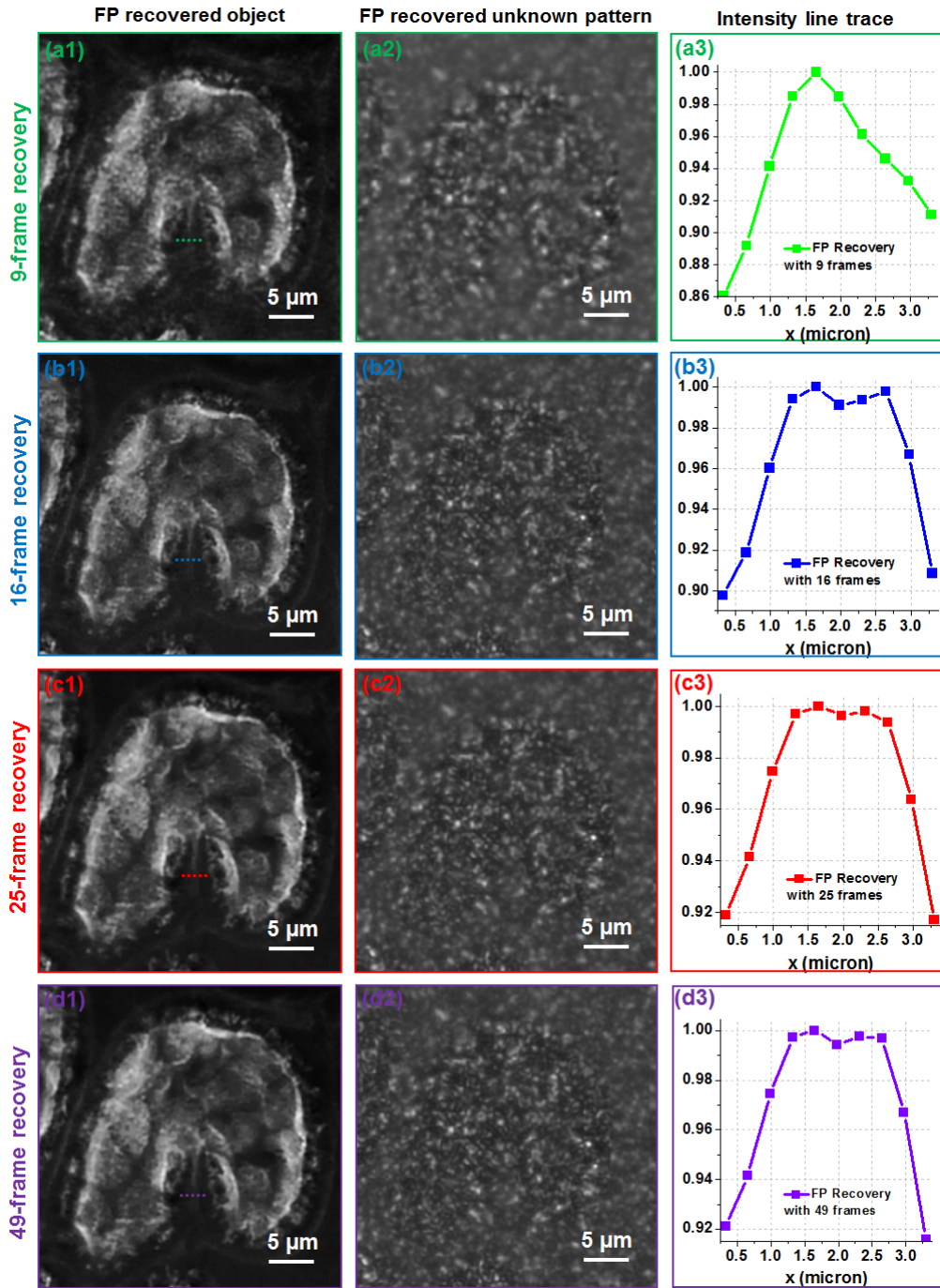


Fig. 13. FP reconstructions using different number of raw images. We used 5-15 loops for the iterative recovery process. (a) 9-frame recovery. (b) 16-frame recovery. (c) 25-frame recovery. (d) 49-frame recovery. (a1)-(d1) The recovered object profiles. (a2)-(d2) The recovered unknown illumination patterns. (a3)-(d3) Intensity lines traces corresponding to the highlighted features in (a1)-(d1). The FP reconstruction converges with 25 raw images.

## 5. Discussion and conclusion

In summary, we have developed and demonstrated an imaging technique, termed pattern-illuminated Fourier ptychography, for high-resolution fluorescence imaging. This approach recovers a high-resolution sample image from many pattern-illuminated low-resolution images. We reiterate that, the use of non-uniform intensity patterns for sample illumination is not a new idea. It has been demonstrated in various imaging settings for improving lateral or axial resolution [2–9, 11–19]. However, the use of the FP framework for recovering a high-resolution fluorescence image is new and may provide an alternative solution for the existing SIM and speckle illuminating platforms.

There are several advantages associated with the reported approach. 1) It is compatible with most existing fluorescence microscope platforms; no major hardware modification is needed. The experimental demonstration presented in this work was performed on a commercially available microscope platform. 2) The rich literatures on correction schemes of FP and conventional ptychography can be integrated into the reported framework. For example, the pupil correction scheme [38] and the adaptive system correction scheme [41] in FP can be integrated into the reported framework for factoring out system uncertainties. The sparsely sampled FP scheme [42] can be used in the reported framework to bypass the pixel aliasing problem. 3) The reported approach is very efficient in terms of computational cost. The solution typically converges with 5-20 loops. In our experimental demonstration, we used 5-15 loops for recovering the images shown in Fig. 12(a1)-(d1). The corresponding computational time is less than one second using an Intel i7 CPU. The reported algorithm is also highly parallelizable. As a result, the computational time can be significantly shortened using a graphical processing unit (GPU). 4) The mechanical scanning range of the reported approach is on the order of speckle size. Therefore, the scanning process is considered very fast compared to the conventional sample scanning process, where the scanning range is on the scale of sample size. In our implementation, the entire scanning region is restricted within 15  $\mu\text{m}$  by 15  $\mu\text{m}$ .

There are three limitations associated with the current experimental setting. 1) The epi-illumination configuration uses the same objective lens for light delivering and light collection. Therefore, it limits the maximum resolution enhancement factor to 2. It would be straight forward to decouple the illumination NA from the collection NA using a transmission configuration. For example, we can use a high-NA condenser lens to produce high-frequency speckle patterns. We can then use a low-NA lens to capture raw images. The final resolution is determined by the high-NA condenser lens while the final field-of-view is determined by the low-NA objective lens. In this regard, it is possible to use the reported approach to develop a high-throughput gigapixel fluorescence imaging platform. Such a development will be complementary to the gigapixel bright-field microscopy using the original FP approach. 2) In the current implementation, the sample scanning positions are assumed to be the known information. This assumption requires the use of precise mechanical stages. However, we note that, it is possible to recover the scanning positions from the cross-correlation of the acquired images. Therefore, it is possible to recover the high-resolution image without knowing the scanning positions of the sample. We will present this result in a future publication. 3) We assume the sample is a 2D section in the reported framework. Modelling the reported FP framework using 3D optical transfer function and 3D speckle patterns is one of our future directions.

## Acknowledgments

We are grateful for the discussion with Dr. Ying Min Wang. For more information on Fourier ptychography, please visit <https://sites.google.com/site/gazheng/>.